12-2013

Monitoring daily evapotranspiration in Northeast Asia using MODIS and a regional Land Data Assimilation System

Keunchang Jang
Kangwon National University

Sinkyu Kang
Kangwon National University

Yoon-Jin Lim

Seungtaek Jeong

Joon Kim

See next page for additional authors

Recommended Citation

Jang, K., S. Kang, Y.-J. Lim, S. Jeong, J. Kim, J. S. Kimball, and S. Y. Hong (2013), Monitoring daily evapotranspiration in Northeast Asia using MODIS and a regional Land Data Assimilation System, J. Geophys. Res. Atmos., 118, 12,927–12,940, doi:10.1002/2013JD020639

Monitoring daily evapotranspiration in Northeast Asia using MODIS and a regional Land Data Assimilation System

Keunchang Jang,[1] Sinkyu Kang,[1] Yoon-Jin Lim,[2] Seungtaek Jeong,[1] Joon Kim,[3] John S. Kimball,[4] and Suk Young Hong[5]

Received 26 July 2013; revised 10 October 2013; accepted 4 November 2013; published 9 December 2013.

[1] We applied an approach for daily estimation and monitoring of evapotranspiration (ET) over the Northeast Asia monsoon region using satellite remote sensing observations from the Moderate Resolution Imaging Spectroradiometer (MODIS). Frequent cloud cover results in a substantial loss of remote sensing information, limiting the capability of continuous ET monitoring for the monsoon region. Accordingly, we applied and evaluated a stand-alone MODIS ET algorithm for representative regional ecosystem types and an alternative algorithm to facilitate continuous regional ET estimates using surface meteorological inputs from the Korea Land Data Assimilation System (KLDAS) in addition to MODIS land products. The resulting ET calculations showed generally favorable agreement (root-mean-square error $< 1.3\ \mathrm{mm\ d^{-1}}$) with respect to in situ measurements from eight regional flux tower sites. The estimated mean annual ET for 3 years (2006 to 2008) was approximately $362.0 \pm 161.5\ \mathrm{mm\ yr^{-1}}$ over the Northeast Asia domain. In general, the MODIS and KLDAS-based ET (MODIS-KLDAS ET) results showed favorable performance when compared to tower observations, though the results were overestimated for a forest site by approximately 39.5% and underestimated for a cropland site in South Korea by 0.8%. The MODIS-KLDAS ET data were generally underestimated relative to the MODIS (MOD16) operational global terrestrial ET product for various biome types, excluding cropland; however, MODIS-KLDAS ET showed better agreement than MOD16 ET for forest and cropland sites in South Korea. Our results indicate that MODIS ET estimates are feasible but are limited by satellite optical-infrared remote sensing constraints over cloudy regions, whereas alternative ET estimates using continuous meteorological inputs from operational regional climate systems (e.g., KLDAS) provide accurate ET results and continuous monitoring capability under all-sky conditions.

Citation: Jang, K., S. Kang, Y.-J. Lim, S. Jeong, J. Kim, J. S. Kimball, and S. Y. Hong (2013), Monitoring daily evapotranspiration in Northeast Asia using MODIS and a regional Land Data Assimilation System, *J. Geophys. Res. Atmos.*, *118*, 12,927–12,940, doi:10.1002/2013JD020639.

1. Introduction

[2] A better understanding of the hydrological cycle requires improved quantification of such water budget components as precipitation, evapotranspiration, runoff, ground water, and soil moisture. Evapotranspiration (ET) quantifies the land and atmosphere exchange of water and latent energy and is the primary link between the global water and energy cycles. ET is one of the main factors in the hydrologic cycle, returning more than 60% of land surface precipitation back to the atmosphere [*Dingman*, 1994; *Oki and Kanae*, 2006; *Trenberth et al.*, 2007]. Therefore, spatially and temporally accurate ET monitoring can provide critical information to improve our understanding of the energy, water, and carbon cycles in terrestrial ecosystems [*Mu et al.*, 2007; *Venturini et al.*, 2008; *Yuan et al.*, 2010].

[3] Satellite remote sensing is a useful technique for estimating and monitoring ET over a large scale because of the global continuity of the observations. Alternative methods for ET estimation and regional monitoring have been developed using satellite remote sensing data, including the NASA Moderate Resolution Imaging Spectroradiometer (MODIS) sensor on Terra and Aqua. The many algorithms to estimate ET using satellite remote sensing data can be separated into purely remote sensing-driven ET algorithms [*Bastiaanssen et al.*, 1998, 2005; *Su*, 2002; *Kim and*

[1]Department of Environmental Science, Kangwon National University, Chuncheon, Korea.
[2]Department of Atmospheric Sciences, Yonsei University, Seoul, Korea.
[3]Department of Landscape Architecture and Rural Systems Engineering, Seoul National University, Seoul, Korea.
[4]Flathead Lake Biological Station, Division of Biological Sciences, University of Montana, Polson, Montana, USA.
[5]Department of Agricultural Environment, National Academy of Agricultural Science, Suwon, Korea.

Corresponding author: S. Kang, Department of Environmental Science, Kangwon National University, Chuncheon 200–701, Korea. (kangsk@kangwon.ac.kr)

2169-897X/13/10.1002/2013JD020639

Hogue, 2008; *Renzullo et al.*, 2008; *Venturini et al.*, 2008; *Jang et al.*, 2009; *Tang et al.*, 2009] and hybrid-type ET algorithms that use remote sensing observations and additional inputs from meteorological reanalysis data [*Boegh et al.*, 2004; *Yang et al.*, 2006; *Cleugh et al.*, 2007; *Mu et al.*, 2007, 2009; *Wang and Georgakakos*, 2007; *Jang et al.*, 2010; *Yuan et al.*, 2010]. The historical methods and accuracy of estimating ET using either in situ measurements or remotely sensed data are comprehensively reviewed by *Glenn et al.* [2007], *Kalma et al.* [2008], and *Li et al.* [2009].

[4] Methods for estimating ET using MODIS data have been developed in several different formulations. In particular, the revised Remote Sensing-Penman Monteith (RS-PM) algorithm proposed by *Mu et al.* [2007] has been used in various studies for estimating ET [*Jang et al.*, 2009, 2010; *Mu et al.*, 2009; *Jeong et al.*, 2009; *Sheffield et al.*, 2009; *Ferguson et al.*, 2010; *Lu and Zuang*, 2010; *Yuan et al.*, 2010]. The revised RS-PM algorithm accounts for both canopy transpiration and soil evaporation components and considers vegetation canopy conductance and environmental constraints (i.e., minimum air temperature, T_{min}, and vapor pressure deficit, VPD) for estimating ET. *Sheffield et al.* [2009] applied the revised RS-PM algorithm for investigating the terrestrial water budget, and *Lu and Zuang* [2010] used the same algorithm to estimate water use efficiency, defined as the ratio of gross primary product to ET, in the conterminous United States; these authors compared MODIS-based ET estimates with in situ tower observations from 28 AmeriFlux sites and found favorable agreement ($r^2 > 0.51$). *Ferguson et al.* [2010] estimated ET using a remotely sensed data set with the revised RS-PM algorithm over the continental U.S. and investigated retrieval bias according to the input sources of ET derived from the variable infiltration capacity, North American Regional Reanalysis, and Gravity Recovery and Climate Experiment. *Jang et al.* [2010] proposed a methodology for estimating ET based on the revised RS-PM algorithm with the MODIS atmosphere and land products over the Geum River basin in South Korea. ET was derived only using MODIS products under clear-sky conditions. Under cloudy-sky conditions, however, meteorological data were obtained from four-dimensional data assimilation [*Dudhia et al.*, 2005] between the MODIS atmospheric product and fifth-generation Mesoscale Meteorological Model to estimate ET because meteorological variables from the MODIS atmosphere products were not available due to cloud contamination.

[5] Regional assessment and continuous daily monitoring of ET over the Northeast Asia monsoon region, constituting various land cover types and complex terrain, is particularly challenging due to frequent and extensive cloud cover, which degrades satellite optical-infrared sensor capabilities for continuous monitoring [*Kang et al.*, 2005; *Zhao et al.*, 2005; *Jang et al.*, 2009]. Satellite observations of land surface conditions are particularly problematic during the summer monsoon season (June to August) due to extensive cloud cover and rainfall, typically causing significant gaps in optical-infrared sensor data. For this reason, ET estimation approaches have used additional ancillary data inputs and meteorological or radiative transfer models to overcome the limitations of the satellite observational data [*Nishida et al.*, 2003; *Yang et al.*, 2006; *Wang and Georgakakos*, 2007; *Mu et al.*, 2009; *Zhang et al.*, 2009; *Jang et al.*, 2010; *Yuan et al.*, 2010].

[6] Global-scale meteorological data are not adequate for many regional applications due to their relatively coarse spatial resolution. For example, the operational MODIS (MOD16) ET product uses MODIS-derived vegetation canopy cover information with coarse- (~1° resolution) scale ancillary surface meteorology inputs from Global Modeling and Assimilation Office (GMAO) reanalysis data to estimate the global daily ET [*Mu et al.*, 2007, 2011]. The NASA Data Assimilation Office and National Centers for Environmental Prediction have even coarser ($1° \times 1.25°$ and $2.5° \times 2.5°$) spatial resolutions. Although the North American Land Data Assimilation System (NLDAS) has higher 0.125° (approximately 10 km) data, it is confined to the North America domain. Recently, *Kim et al.* [2012] reported on validation errors of MOD16 ET products using 17 flux tower observation sites in East Asia and found considerable errors for MOD16A2 8 day ET retrievals at all sites, with the largest error for grassland sites. These authors concluded that the characteristics of climate and topography in Asia should be considered because the Asian region has complex terrain, land cover, and land use. Therefore, for regional applications, finer-scale meteorological data can better resolve local spatial heterogeneity in surface meteorology and associated ET patterns.

[7] In this study, the methodology proposed by *Jang et al.* [2010] was applied to monitor daily ET over Northeast Asia by combining MODIS products and regional meteorological data from the Korea Land Data Assimilation System (KLDAS), a regional LDAS application that provides improved spatial resolution (10×10 km) with an hourly time step over Northeast Asia [*Lim et al.*, 2010]. The objectives of the present study are to quantify the regional patterns and daily variability of ET over the Northeast Asia monsoon region and to determine the underlying environmental factors controlling these processes. We used a stand-alone MODIS ET algorithm [*Jang et al.*, 2010] under clear and partially cloudy conditions, applying the same algorithm using KLDAS and MODIS drivers for cloudy-sky conditions to facilitate continuous daily ET estimates. The ET simulations are evaluated using in situ tower eddy covariance flux measurements from regionally representative land cover types.

2. Materials and Methods

2.1. Study Sites and Data Collection

[8] The Northeast Asia region including South and North Korea, Japan, eastern China, and Mongolia was selected as the study domain (as denoted by the red box in Figure 1). This domain encompasses an area of ~7,681,000 km^2, ranging from 100 to 150°E longitude and 30 to 50°N latitude, and represents a major portion of the Asian monsoon region. The annual precipitation is higher (1600–2200 mm) in the southern and eastern parts of the domain due to the summer monsoon, which extends in a southwest to northeast trajectory across the region. The southern portion of the domain is relatively hot and humid, with annual precipitation exceeding 2000 mm, whereas the northwest portion of the domain is very dry, with annual precipitation less than 300 mm. Grassland and barren areas are distributed throughout the dry northwestern parts of the domain, and forests, including

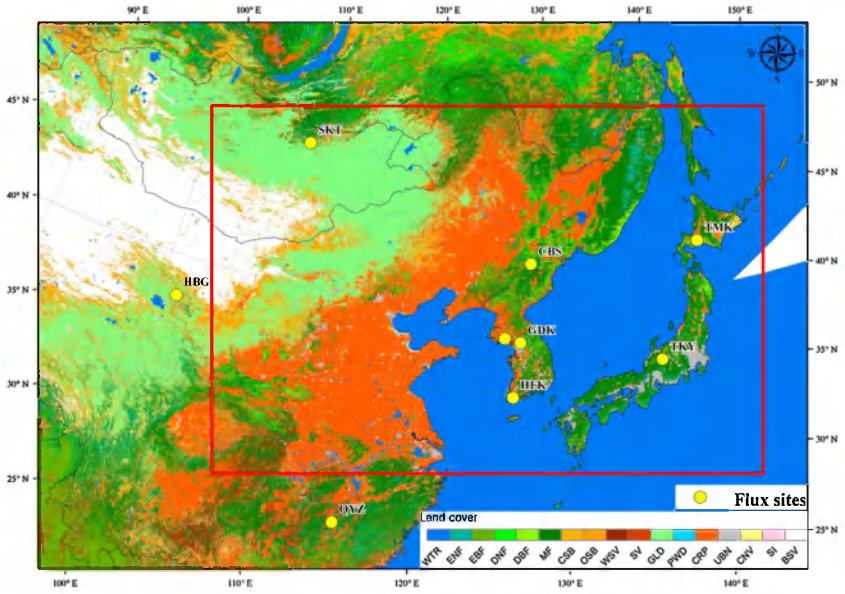

Figure 1. Land cover map produced from the MODIS (MOD12Q1) land cover product and the distribution of the flux tower measurement sites (yellow dots). The Northeast Asia study domain and associated ET simulations are indicated by the red box.

mixed forest, deciduous broadleaf forest, and evergreen needleleaf forest, are the major vegetation type in the eastern portion of the domain (Figure 1). Major cropland areas are distributed over the central portion of the domain; in the southern areas, rice and sorghum are major crops, and corn and wheat are cultivated in the northeastern part of China.

[9] We obtained observational data from eight eddy covariance flux measurement towers in East Asia. These observational data (e.g., see Table 1 and the yellow circles in Figure 1) were used to evaluate MODIS remote sensing-based meteorological variables and validate the ET retrievals derived from the MODIS stand-alone algorithm. The flux towers used in this investigation are located in Korea (two sites; GDK and HFK), Japan (two sites; TKY and TMK), Mongolia (one site; SKT), and China (three sites; CBS, HBG, and QYZ), which represent various major regional vegetation types, including broadleaf deciduous forest, evergreen coniferous forest, mixed (deciduous and coniferous) forest, grassland, and cropland (Table 1).

2.2. Description of the ET Algorithm

[10] The Penman-Monteith (PM) equation [*Penman*, 1948; *Monteith*, 1965; *Monteith and Unsworth*, 1990] has frequently been used in hydrological, agricultural, and

Table 1. Description of Study Sites

Site Name	Location (°N, °E)	Elevation (m)	Temperature[a] (°C)	Precipitation[a] (mm)	Local Dominant Species	Land Cover Type	Tree Age (years)	LAI[b] ($m^2 m^{-2}$)	Study Period[c]	References
GDK (Gwangneung)	37. 76, 127.15	340	11.5	1332	*Quercus* sp., *Carpinus* sp.	MF	80–200	6	2004289–2006365	*Kim et al.* [2006]
HFK (Haenam)	34.55, 126.57	13	13.3	1306	Seasonally cultivated crops (paddy rice, bean, sweet potato, Indian millet, and sesame)	CRP	1	3	2004001–2006365	*Lee et al.* [2003]
TKY (Takayama)	36.15, 137.42	1420	6.5	2275	*Betula*, *Quercus* sp.	DBF	50	4	2002001–2004365	*Saigusa et al.* [2008, 2010]
TMK (Tomakomai)	42.74, 141.52	140	6.2	1043	*Larix kaempferi*, *Betula ermanii*	BNF	45	5.6	2002001–2003365	*Hirata et al.* [2008]
CBS (Changbaishan)	42.40, 128.08	738	3.6	695	*Pinus koraiensis*, *Tilia amurensis*	MF	200	6.1	2003001–2004365	*Yu et al.* [2007]
QYZ (Qianyanzhou)	26.73, 115.05	102	17.9	1485	*Pinus* sp., *Cunninghamia lanceolata*	ENF	21	3.5	2003001–2004365	*Yu et al.* [2007, 2008]
HBG (Haibei)	37.66, 101.33	3200	−1.7	600	*Kobresia tibetica*, *Carex* sp.	GLD	-	4	2003001–2004365	*Zhongmin et al.* [2009]
SKT (Southern Khentei Taiga)	48.35, 108.65	1630	−2.9	282	*Carex Spp.*, *Koeleria spp.*, *Larix sibirica*	DNF	70–150	2.7	2003001–2005365	*Li et al.* [2005]

[a]The mean annual air temperature and precipitation from the AsiaFlux website (http://www.asiaflux.net/).
[b]The maximum LAI (projected).
[c]The data period used in this study.

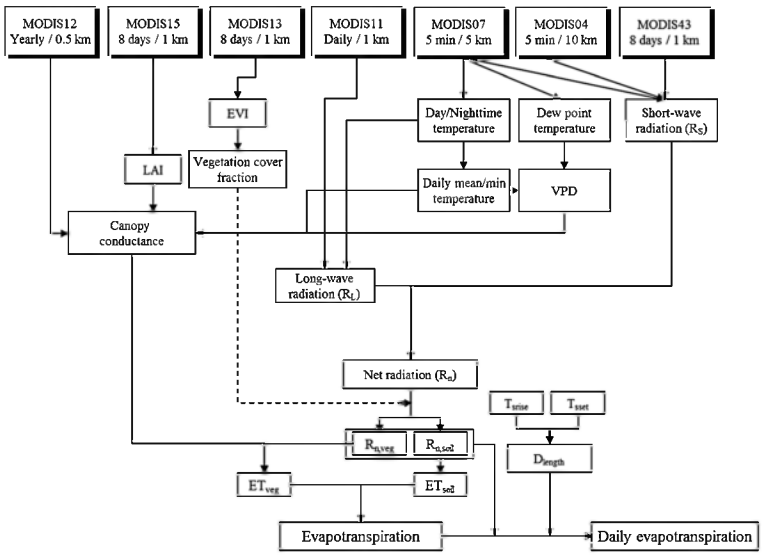

Figure 2. Processing flow for estimating ET using MODIS atmosphere and land products.

natural vegetation studies to estimate ET for a variety of hydroclimatic regimes [*Nishida et al.*, 2003; *Cleugh et al.*, 2007; *Mu et al.*, 2007; *Wang and Georgakakos*, 2007; *Sheffield et al.*, 2009; *Jang et al.*, 2010; *Yuan et al.*, 2010]. The revised RS-PM algorithm [*Mu et al.*, 2007] is a modified version of the RS-PM algorithm proposed by *Cleugh et al.* [2007] and has been used in various applications [*Mu et al.*, 2007, 2009; *Jang et al.*, 2009, 2010; *Sheffield et al.*, 2009; *Yuan et al.*, 2010]. We used the same ET estimation algorithm as *Jang et al.* [2010], who modified the surface resistance estimation in the revised RS-PM algorithm from *Mu et al.* [2007] by considering the maximum leaf conductance (C_L) for various biome types, by adding a shelter effect term (f_s) that accounts for the sheltering effect caused by canopy phenology changes [*Dingman*, 1994], and by considering atmospheric conditions that are determined by the presence of clouds. This approach uses a modified form of the *Mu et al.* [2007] algorithm, utilizing only MODIS land and atmosphere inputs to estimate ET during clear or partial cloud cover conditions (Figure 2); an alternative implementation scheme is applied for cloudy-sky conditions using additional ancillary surface meteorology inputs from model data assimilation. The latent heat flux (λE) term is composed of canopy transpiration (λE_{veg}) and soil evaporation ($\lambda E_{\mathrm{soil}}$) components (Table 2).

Table 2. ET Model Parameters and Equations

Parameter	Description	Equation		References
λE	Total evapotranspiration	$\lambda E_{veg}+\lambda E_{soil}$		*Mu et al.* [2007]
λE_{veg}	Canopy transpiration	$\frac{\Delta R_{n,cano}+\rho c_p(e_s-e_a)/r_a}{\Delta+\gamma(1+r_s/r_a)}$		*Mu et al.* [2007]
$\lambda E_{\mathrm{soil}}$	Soil evaporation	$\frac{\Delta R_{n,soil}+\rho c_p(e_s-e_a)/r_a}{\Delta+\gamma(r_{tot}/r_a)}\left(\frac{RH}{100}\right)^{(e_s-e_a)/100}$		*Mu et al.* [2007]
g_c	Stomatal conductance	$C_L\times m(T_{min})\times m(VPD)$		*Jang et al.* [2010]
C_c	Canopy conductance	$g_c\times LAI\times f_s$		*Jang et al.* [2010]
f_s	Shelter factor	$f_{s_{open}}+\frac{(LAI-LAI_{min})\times\left(f_{s_{close}}-f_{s_{open}}\right)}{LAI_{max}-LAI_{min}}$	$0\le LAI<3$	*Jang et al.* [2010]
r_s	Surface resistance	$f_{s_{close}}$	$LAI\ge 3$	*Mu et al.* [2007]
		$1/C_c$		
r_a	Aerodynamic resistance	$(rc\times rr)/(rc+rr)$		*Mu et al.* [2009]
r_r	Resistance to radiative heat transfer	$\frac{\rho c_p}{4.0\times\sigma\times(T_a+273.15)^3}$		*Mu et al.* [2007]
r_c	Resistance to convective heat transfer	$r_{totc}\times r_{corr}$		*Mu et al.* [2007]
r_{corr}	Correction coefficient for the total aerodynamic resistance to vapor transport	$\left[\left(\frac{T_a+273.15}{293.15}\right)^{1.75}\times\left(\frac{101300}{P_1}\right)\right]^{-1}$		*Jones* [1992] and *Mu et al.* [2007]
DANR	Daily average net radiation	$\frac{\int_{t_{rise}}^{t_{set}}R_n(t)dt}{\int_{t_{rise}}^{t_{set}}dt}=\frac{2R_n}{\pi\sin\left[\left(\frac{t_{overpass}-t_{rise}}{t_{set}-t_{rise}}\right)\pi\right]}$		*Bisht et al.* [2005]
DET	Daily ET	$(DANR\times D_{length})\times\left(\frac{IET}{R_n}\right)\times\frac{0.0036}{2.5}$		*Jang et al.* [2010]

[11] The ET algorithm considers the effects of surface energy-partitioning processes and environmental constraints, including the daily minimum air temperature (T_{min}) and vapor pressure deficit (VPD; i.e., $e_s - e_a$), on stomatal conductance and ET [*Mu et al.*, 2007, 2009]. As a key parameter for estimating ET, the surface net radiation (R_n, W m^{-2}) was calculated using MODIS atmosphere and land products [*Jang et al.*, 2010]. The stomatal conductance (g_c) was estimated using the maximum leaf conductance (C_L), defined as the mean potential stomatal conductance per unit leaf area [*Federer et al.*, 1996], and was reduced for unfavorable T_{min} and VPD conditions [*Mu et al.*, 2007; *Yuan et al.*, 2010]. The surface resistance (r_s) is equal to the inversion of canopy conductance (C_c), which was calculated using g_c, leaf area index (LAI), and the shelter factor (f_s). A biome property look-up table (BPLUT) was used to define the range of environmental constraints for various land cover types [*Mu et al.*, 2007, 2009; *Jang et al.*, 2009, 2010]. The aerodynamic resistance (r_a), which strongly influences ET, was estimated by following *Mu et al.* [2007] using MODIS atmosphere and land products; this calculation was adopted in previous studies, including *Zhang et al.* [2009], *Jang et al.* [2010], and *Jeong et al.* [2009]. Details of the equations for aerodynamic resistance can be found in *Mu et al.* [2007] and are presented in Table 2.

[12] The main differences from *Jang et al.* [2010] are the change of input variables, including LAI and the enhanced vegetation index (EVI) as well as meteorological inputs. The previous study used the MODIS MYD13A2 vegetation index product to estimate LAI as an input for ET estimation. In the current study, LAI data were obtained directly from the MODIS MYD15A2 LAI product, which employs a detailed radiative transfer modeling approach for LAI estimation that accounts for canopy architecture effects on vegetation radiation absorption. The temporal resolution of EVI, which was used to calculate the vegetation cover fraction, was enhanced from 16 days to 8 days by integrating Terra and Aqua MODIS (MOD13A2 and MYD13A2) EVI products. More detailed introduction and preprocessing for MODIS products are presented in section 2.4 and *Jang et al.* [2010]. The meteorological inputs were obtained from KLDAS, including the surface air temperature (T_a), relative humidity (RH), surface air pressure (P_1), and downward shortwave radiation ($R_S^{\downarrow}$) to estimate ET under cloudy-sky conditions. However, R_n, which is required for estimating ET, was not produced in KLDAS. For this reason, we estimated R_n using the relationships between $R_S^{\downarrow}$ and R_n for each of major biome types. More detailed descriptions for KLDAS data are presented in section 2.5.

[13] The daily ET (DET, mm d^{-1}) is generally more useful for hydrological applications than the instantaneous ET (IET or λE, W m^{-2}) derived at the satellite overpass time. *Jang et al.* [2010] suggested a methodology to scale IET to estimate DET based on the assumptions that the diurnal net radiation (R_n) variation follows a sinusoidal pattern and that the evaporation fraction (EF), defined as the ratio of λE (i.e., IET) to available energy (i.e., R_n) [*Shuttleworth et al.*, 1989], is relatively constant during the daytime. The assumption of conservative EF diurnal variability is supported by previous research [*Sugita and Brutsaert*, 1991; *Crago and Brutsaert*, 1996]. The sinusoidal model was employed, and the day length (D_{length}) was calculated as suggested by *Dingman* [1994] and utilized, together with EF, to estimate daily ET.

2.3. MODIS-KLDAS ET

[14] We used a similar processing scheme as *Jang et al.* [2010] to estimate DET over Northeast Asia; this method used cloud mask information from the MODIS atmosphere profile product. In this study, the number of clear atmosphere pixels (ClearPix) derived from MODIS (MOD07_L2 product) was used to determine sky conditions within each 5×5 km resolution atmosphere pixel (i.e., 25 MODIS 1 km land pixels). A ClearPix value of 25 indicates completely clear-sky conditions within a given atmosphere pixel; ClearPix values less than 5 were considered severely cloudy, and subsequently, other atmospheric data were not produced.

[15] For clear to partially clear-sky conditions (ClearPix ≥ 5), DET was estimated using MODIS products with the processing scheme presented in Figure 2. Under cloudy conditions (ClearPix < 5), ancillary meteorological inputs were obtained from KLDAS, including T_a, RH, P_1, and $R_S^{\downarrow}$. Because KLDAS does not provide net radiation data, we devised a simple regression method to estimate R_n from $R_S^{\downarrow}$. A more detailed description is provided in section 2.5.

[16] Consequently, the DET estimation was performed solely using MODIS product inputs under clear to partially clear-sky conditions (MODIS ET; Figure 2) or using additional ancillary surface meteorological inputs from KLDAS under MODIS-defined cloudy conditions (KLDAS ET). The MODIS and KLDAS ET results were then combined (MODIS-KLDAS ET) for spatially and temporally continuous mapping of ET over the Northeast Asia domain.

2.4. MODIS Data

[17] Several MODIS land and atmosphere products were used to estimate MODIS ET at 1 km spatial resolution. Similar MODIS products have been used to estimate the terrestrial radiation budget [*Bisht et al.*, 2005; *Ryu et al.*, 2008; *Bisht and Bras*, 2010], ET [*Mu et al.*, 2007, 2009; *Jang et al.*, 2009, 2010], and vegetation gross primary productivity [*Zhao et al.*, 2005; *Yuan et al.*, 2010; *Zhao and Running*, 2010]. In this study, we used several of the Collection 5 Aqua MODIS land and atmosphere products to estimate ET, including the MYD11A1 land surface "skin" temperature and emissivity, MOD12Q1 land cover classification, MYD15A2 LAI, MCD43B3 albedo, and atmospheric products (MYD04_L2 aerosol and MYD07_L2 atmospheric profiles). EVI data were obtained from Terra and Aqua MODIS (MOD13A2 and MYD13A2) products to calculate the vegetation cover fraction. *Jang et al.* [2010] discussed the problem of the coarse temporal resolution (16 day) of vegetation indices. For this reason, we integrated the EVI data using the 16 day products available from the Terra and Aqua product streams to improve EVI temporal fidelity (8 day) for ET estimation.

[18] Cloud contamination of satellite optical-infrared remote sensing retrievals is a major cause of reduced data quality and low retrieval rates over many areas of the globe [*Kang et al.*, 2005; *Zhao et al.*, 2005; *Mu et al.*, 2007; *Jang et al.*, 2010]. *Jang et al.* [2010] successfully applied gap-filling techniques for MODIS aerosol, vegetation indices, and albedo inputs to improve the downstream retrieval rates for shortwave radiation ($R_S^{\downarrow}$), which is a fundamental variable for the estimation of R_n and ET; we applied these same techniques to estimate ET in the present study.

[19] The MOD16A2 ET product, which is an 8 day cumulative ET generated by the improved RS-PM ET algorithm [*Mu et al.*, 2011], was used to compare the spatial variability of ET over Northeast Asia. The improved RS-PM algorithm is the version modified by *Mu et al.* [2007], simplifying the calculation of vegetation fractional cover and considering both daytime and nighttime ET, adding a soil heat flux term, separating dry canopy surface from wet, and dividing the soil surface into saturated wet and drier moisture components. *Mu et al.* [2011] also calibrated a BPLUT for the best estimation of ET and reported favorable agreement in comparison to flux tower observations from AmeriFlux sites.

2.5. Korea Land Data Assimilation System (KLDAS)

[20] The Land Data Assimilation System (LDAS) is a land surface initialization technique to improve weather and climate prediction. There are several LDAS studies at global or regional scales, including the Global LDAS (GLDAS) [*Rodell et al.*, 2004], the North American LDAS (NLDAS) [*Mitchell et al.*, 2004], the South American LDAS (SALDAS) [*de Goncalves et al.*, 2006], and the High Resolution LDAS [*Chen et al.*, 2009]. KLDAS, which follows the concept and methodology used in many LDAS projects, was developed over East Asia by integrating a physically based land process model with satellite remote sensing and ground-based observation data [*Lim et al.*, 2010]. KLDAS is essentially an offline Noah land surface model (LSM) system [*Ek et al.*, 2003] uncoupled from an atmospheric model that integrates various data, including satellite-based land cover, time-variable vegetation characteristics and downward shortwave solar radiation, and observed rainfall and modeled near-surface meteorological variables. The purpose of KLDAS is to improve land surface parameters of the offline Noah LSM by producing realistic data sets over East Asia (between 10 to 50°N and 110 to 155°E). *Lim et al.* [2010] processed two data fields: (1) analysis-based fields (i.e., air and dew point temperatures and wind components) that were bilinearly interpolated from 0.5625° and 6-hourly data from Global Data Assimilation and Prediction System analysis fields to 10 km spatial resolution and hourly timescales and (2) observation-based fields, including precipitation and downward shortwave radiation, produced from geostationary satellite data such as GOES 9, MTSAT-1R and Global Telecommunication System accumulated precipitation, and Automatic Weather System precipitation. *Lim et al.* [2010] utilized MODIS land products, including MODIS MOD12C1 land cover, MOD13C1 EVI, and MOD15 LAI to obtain improved information regarding the land surface status.

[21] Various meteorological data, including T_a, RH, P_1, and $R_S^{\downarrow}$, have been generated from KLDAS over the East Asia domain, with 10 km spatial resolution and hourly temporal fidelity. These data were used in this study, with MODIS land products, to estimate ET (i.e., KLDAS ET) when MODIS ET was not produced due to cloud contaminated pixels. However, because the net radiation (R_n) inputs required for estimating ET are not produced in KLDAS, we applied a simple regression method to estimate R_n using the relationships established between the observed $R_S^{\downarrow}$ and R_n for each of the major biome types in the study domain. The simple linear regression models used to estimate R_n from $R_S^{\downarrow}$ were reported in several previous studies [*Kaminsky and Dubayah*, 1997; *Alados et al.*, 2003; *Kwon*, 2009]. The commonly used equations can be expressed as follows:

$$R_n = a_1 R_S^{\downarrow} + b_1 \tag{1}$$

$$R_n = a_1(1\text{-}\alpha) R_S^{\downarrow} + b_1 \tag{2}$$

where a_1 and b_1 are biome-specific regression coefficients and α is the albedo obtained from the MODIS MCD43B3 product.

[22] *Alados et al.* [2003] explored these relationships using 38 months of 5 min resolution surface radiation data over sparse shrubland in Spain and concluded that the simple regression method (equations (1) and (2)) provides a reasonable estimation of R_n. *Kwon* [2009] investigated the relationship between R_n and $R_S^{\downarrow}$ using equation (1) for three major plant functional types (deciduous forest, coniferous forest, and farmland) in Korea and reported different values of a_1 and b_1 for each type. In the present study, the KLDAS-based R_n was estimated using equation (2), and the coefficients (a_1 and b_1) were obtained for individual biome types using linear regression analysis. For clear and partially clear-sky conditions, the coefficients were developed using $R_S^{\downarrow}$ and R_n data from MODIS; for cloudy conditions, we applied the biome-specific regression model to estimate R_n from the KLDAS-derived $R_S^{\downarrow}$.

3. Results

3.1. Validation of Input Variables

3.1.1. MODIS Inputs

[23] The MODIS product inputs were compared with ground-based measurements from flux tower sites representing the major biome types within the domain (Table 3). The MYD07_L2-based air temperature (T_a) retrievals under clear-sky conditions showed favorable agreement with surface air temperature measurements from the eight flux tower sites. The coefficient of determination (r^2), mean residual error (ME), and root-mean-square error (RMSE) metrics describing these relationships ranged from 0.82 to 0.94, from −6.9 to +1.1°C, and from 2.4 to 7.8°C, respectively. The HBG site showed good agreement ($r^2 = 0.82$) between the MODIS- and tower-based temperatures, whereas the ME (−6.9°C) and RMSE (7.8°C) metrics describing these relationships were larger than those of other sites. The error ranges were generally similar to those reported from previous studies [*Bisht et al.*, 2005; *Ryu et al.*, 2008; *Jang et al.*, 2010]. VPD was generally underestimated. Overall, the ME and RMSE values for VPD ranged from −0.73 to +0.10 kPa and from 0.27 to 0.67 kPa, respectively.

[24] The net radiation (R_n; W m^{-2}) and its components, including downward and upward shortwave ($R_S^{\downarrow}$ and $R_S^{\uparrow}$; W m^{-2}) and longwave radiations ($R_L^{\downarrow}$ and $R_L^{\uparrow}$; W m^{-2}), agreed well with the flux tower measurements; $R_S^{\downarrow}$ showed good agreement ($r^2 \geq 0.83$) with the flux tower measurements except for the HBG site ($r^2 = 0.67$); $R_S^{\downarrow}$ was slightly underestimated at all sites, though the associated RMSE differences were less than 120 W m^{-2}. The $R_S^{\uparrow}$, $R_L^{\downarrow}$, and $R_L^{\uparrow}$ results also showed good agreement when compared to the

Table 3. Error Statistics for the T_a, VPD, $R_S^{\downarrow}$, $R_S^{\uparrow}$, $R_L^{\downarrow}$, $R_L^{\uparrow}$, and R_n Measurements at the Eight Tower Sites for the Study Period Presented in Table 1[a]

	ME/RMSE (r^2)						
Site ID	T_a (°C)	VPD (kPa)	$R_S^{\downarrow}$ (W m^{-2})	$R_S^{\uparrow}$ (W m^{-2})	$R_L^{\downarrow}$ (W m^{-2})	$R_L^{\uparrow}$ (W m^{-2})	R_n (W m^{-2})
GDK	−0.3/3.5 (0.94)	−0.2/0.3 (0.90)	−33.0/69.1 (0.88)	-	-	-	−43.8/67.1 (0.94)
HFK	−0.4/2.5 (0.93)	−0.2/0.4 (0.71)	−38.0/53.7 (0.94)	-	-	-	+35.9/46.2 (0.95)
TKY	−0.7/2.4 (0.91)	+0.1/0.3 (0.53)	−38.3/94.2 (0.90)	−29.4/35.5 (0.85)	−36.1/44.0 (0.67)	−26.2/30.9 (0.89)	−25.2/56.5 (0.90)
TMK	−2.5/3.2 (0.91)	−0.1/0.3 (0.45)	−14.2/83.8 (0.85)	−7.7/16.3 (0.81)	−24.7/27.1 (0.92)	−7.6/13.7 (0.93)	−19.1/75.2 (0.84)
CBS	−5.6/6.2 (0.88)	−0.5/0.7 (0.49)	−43.7/81.5 (0.83)	+2.0/12.9 (0.79)	−4.8/56.0 (0.47)	+12.2/57.2 (0.44)	−51.2/103.2 (0.60)
QYZ	+1.1/3.5 (0.84)	−0.0/0.5 (0.62)	−4.1/52.4 (0.84)	+33.4/36.9 (0.20)	+17.1/45.0 (0.77)	+5.1/34.1 (0.96)	−26.0/54.2 (0.86)
HBG	−6.9/7.8 (0.82)	−0.7/0.5 (0.10)	−51.6/114.9 (0.67)	+32.7/35.5 (0.57)	+4.1/28.1 (0.87)	+1.9/18.7 (0.80)	−82.0/115.2 (0.73)
SKT	−1.2/4.2 (0.89)	−0.0/0.3 (0.81)	−40.0/97.1 (0.83)	−4.3/9.5 (0.47)	+32.5/36.6 (0.92)	+45.4/52.7 (0.95)	−90.1/117.5 (0.82)

[a]The ME, RMSE, and r^2 are the mean error, the root-mean-square error, and the determination of coefficient, respectively.

tower site measurements, and the associated RMSE range was less than 60 W m^{-2} at all sites (Table 3). The estimated R_n showed reasonable accuracy, with an r^2 over 0.60, and was generally underestimated at seven sites (ME = −90.1 to −19.1 W m^{-2}), excluding the HFK site (ME = +35.9 W m^{-2}).

3.1.2. KLDAS Inputs

[25] The input variables derived from KLDAS were compared with two flux tower sites in Korea for 2006, i.e., the GDK and HFK sites. The KLDAS-derived T_a showed favorable agreement with surface air temperature measurements

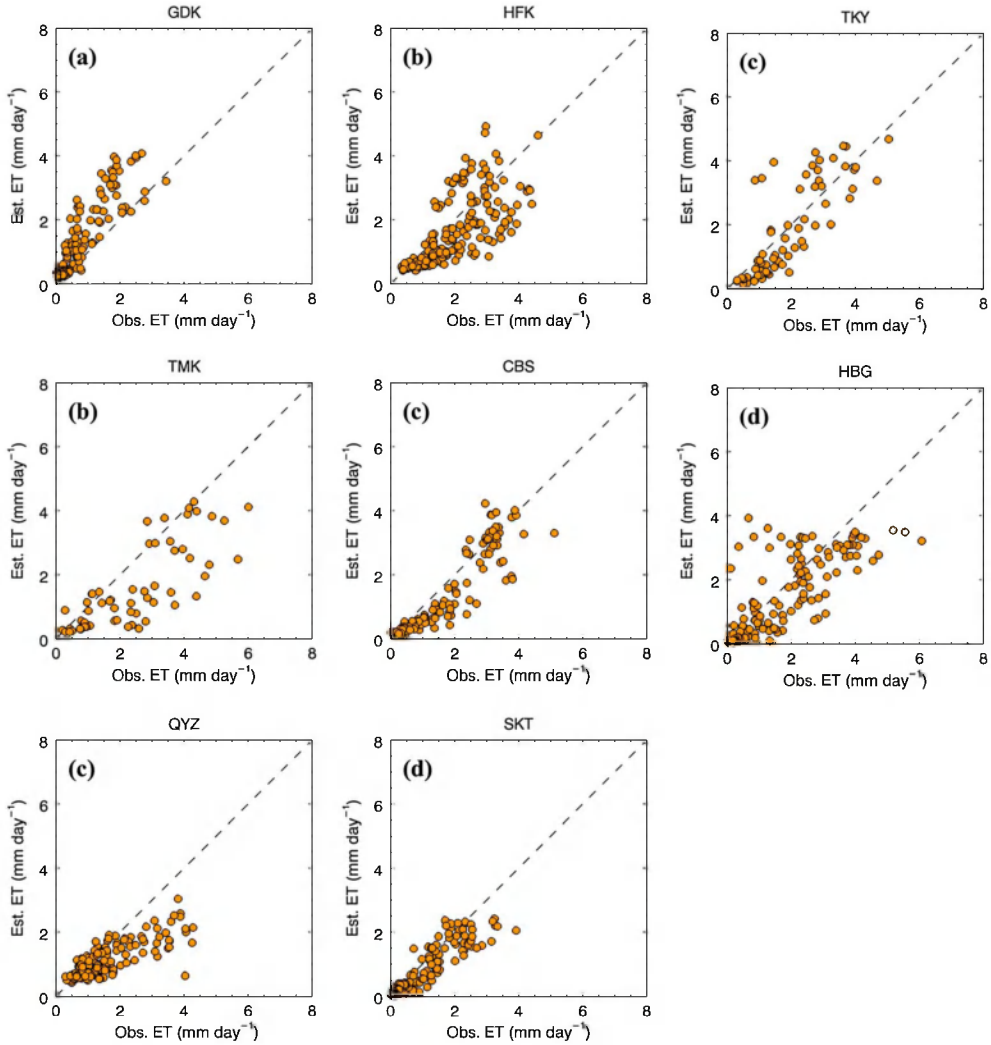

Figure 3. Comparison of the MODIS-based daily ET (mm d^{-1}) with corresponding ET measurements over a 5 year period at the eight flux tower sites: (a) GDK, (b) HFK, (c) TKY, (d) TMK, (e) CBS, (f) HBG, (g) QYZ, and (h) SKT.

Table 4. Error Statistics for the MODIS Instantaneous and Daily ET Results at the Eight Tower Sites

	Instantaneous ET ($W\,m^{-2}$)		Daily ET ($mm\,d^{-1}$)	
Site	r^2	ME (RMSE)	r^2	ME (RMSE)
GDK	0.73	+41.0 (58.9)	0.81	+0.4 (0.7)
HFK	0.33	−35.7 (83.1)	0.48	−0.3 (0.9)
TKY	0.40	−43.2 (118.0)	0.66	−0.1 (0.8)
TMK	0.58	−67.3 (105.3)	0.62	−0.9 (1.3)
CBS	0.66	−35.2 (67.0)	0.82	−0.3 (0.6)
HBG	0.60	−15.7 (66.1)	0.67	−0.2 (0.8)
QYZ	0.45	−81.3 (123.8)	0.61	−0.5 (0.8)
SKT	0.79	−30.7 (49.1)	0.84	−0.2 (0.4)

at the two sites. The r^2, ME, and RMSE values for the GDK and HFK sites were 0.96 and 0.89°C, −1.7 and −1.1°C, and 2.7 and 3.5°C, respectively. VPD was generally underestimated. The ME and RMSE values for VPD were −0.12 (GDK) and −0.14 (HFK) kPa and 0.29 (GDK) to 0.38 (HFK) kPa, respectively. The $R_S^{\downarrow}$ value derived from KLDAS showed favorable agreement with the flux tower measurements; $R_S^{\downarrow}$ was slightly overestimated at the two sites, with +47.9 $W\,m^{-2}$ ME for the GDK site and +35.2 $W\,m^{-2}$ for the HFK site, though the associated RMSE differences were less than 130 $W\,m^{-2}$. The R_n value estimated using equation (2) showed reasonable accuracy; r^2 for the GDK and HFK sites was 0.76 and 0.65, respectively. The R_n ME was slightly overestimated at ME = +13.1 for the GDK site and +41.6 $W\,m^{-2}$ for the HFK site.

3.2. ET Estimates

3.2.1. MODIS ET

[26] The MODIS stand-alone ET results were validated through comparisons with ground-based observations from the eight flux tower sites in the Northeast Asia domain (see Figure 3 and Table 4). The instantaneous ET (IET, $W\,m^{-2}$) at the satellite overpass time was generally underestimated relative to the tower observations, with an ME ranging from −15.6 (HBG) to +41.0 (GDK) $W\,m^{-2}$ and RMSE values ranging from 49.1 (SKT) to 123.8 (QYZ) $W\,m^{-2}$. Low r^2

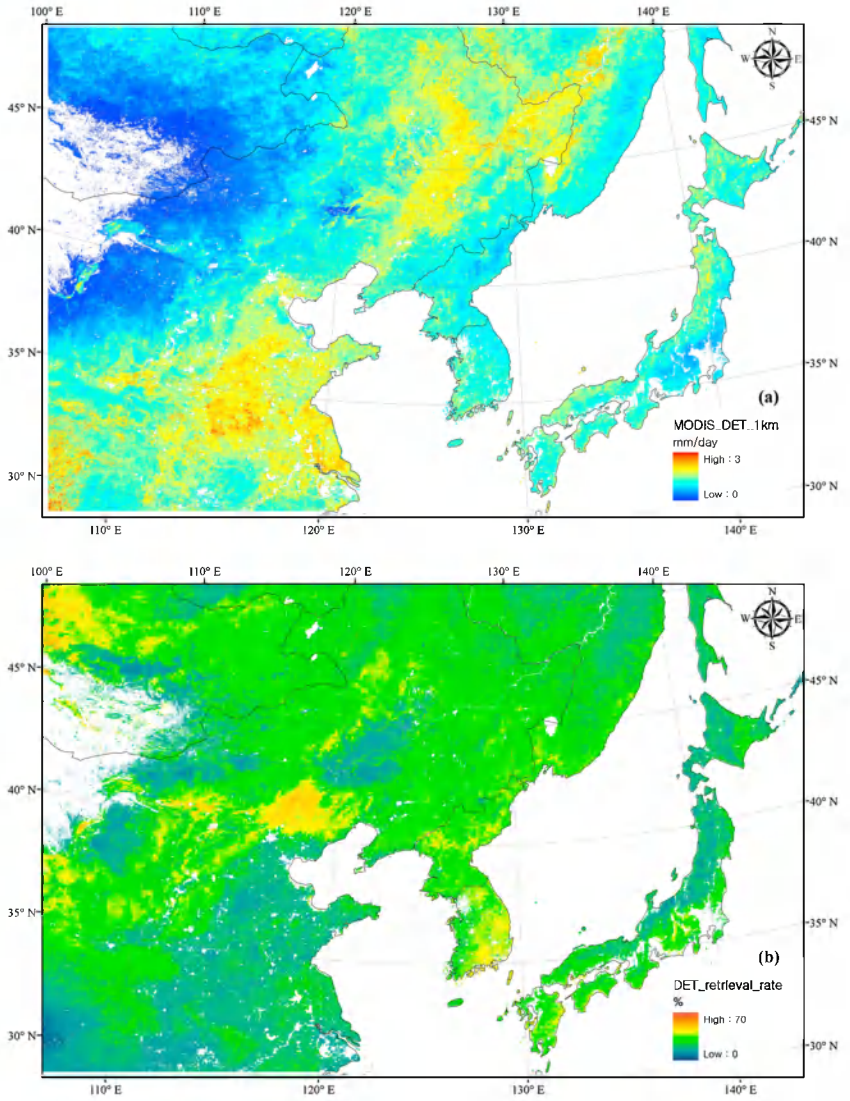

Figure 4. Maps of (a) MODIS-based annual mean ET and (b) the associated retrieval rate in 2006; the retrieval rate is defined as the proportion of successful daily retrievals over the total annual (365 day) period.

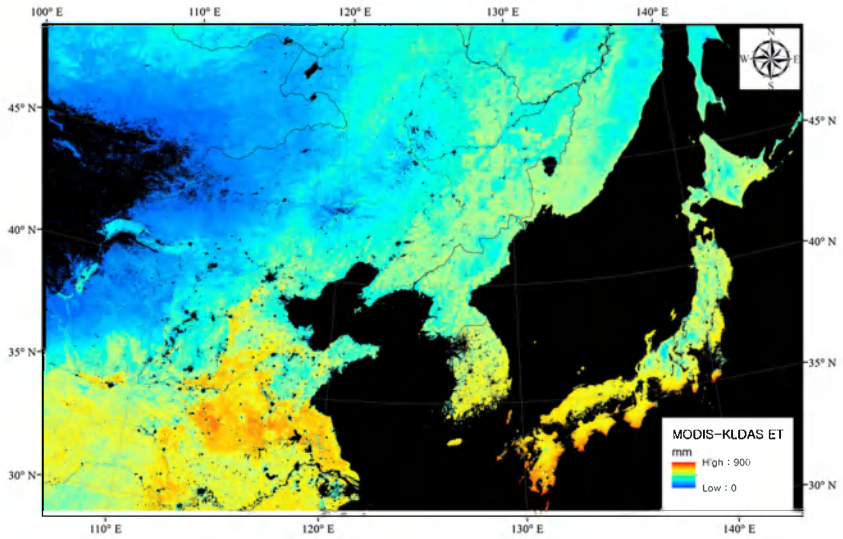

Figure 5. Annual ET (mm yr^{-1}) map from 2006 to 2008 produced by integrating the MODIS ET and KLDAS ET results over the Northeast Asia domain.

values were observed at the HFK (0.33), TKY (0.40), and QYZ (0.45) sites. For the GDK site, the MODIS IET results generally were overestimated in comparison to the flux tower measurements (ME = +41.0 W m^{-2}).

[27] Overall, the MODIS daily ET (DET, mm d^{-1}) showed better agreement with the tower observations (Figure 3) than IET for all sites. Although the result between the MODIS and tower DET showed relatively weak agreement for the HFK site ($r^2 = 0.48$), all other sites showed generally strong agreement ($r^2 > 0.61$) (Table 4). ME and RMSE varied from −0.9 to +0.4 mm d^{-1} and from 0.4 to 1.3 mm d^{-1}, respectively. The MODIS DET results were generally underestimated when compared to the tower observations, with the exception of the GDK site (ME = +0.4 mm d^{-1}). The lowest value of ME (−0.9 mm d^{-1}) was found for the TMK site.

3.2.2. KLDAS ET

[28] The daily-scale KLDAS ET (DET, mm d^{-1}) results were compared to the GDK and HFK tower observations for 2006. KLDAS DET showed good agreement for the GDK site, with $r^2 = 0.78$; ME and RMSE were +0.40 and 0.64 mm d^{-1}, respectively. The KLDAS DET was slightly underestimated for the HFK site, with −0.09 mm d^{-1} of ME; r^2 was 0.67, which was higher than MODIS DET ($r^2 = 0.48$). The KLDAS DET RMSE value at the HFK site was 0.63 mm d^{-1} for 2006.

3.3. MODIS-KLDAS ET

[29] The MODIS stand-alone daily ET resulted in a 35% average retrieval rate for the study domain from 2006 to 2008 (Figure 4). The major gaps were confined to periods from late spring to early autumn. Although the retrieval rate was high over some areas, including central Mongolia, northeastern China, southern Korea, and southern Japan, even these regions showed successful retrievals of less than 60% of the annual cycle. The low retrieval rate was largely due to frequent cloud cover, which strongly degrades satellite optical-infrared remote sensing capability for continuous ET monitoring over Northeast Asia, particularly during the monsoon season.

[30] KLDAS ET was used for the gap-filling of missing data in the MODIS DET record and agreed well with MODIS ET, showing an r^2 that ranged from 0.8936 (ENF) to 0.9749 (DBF). Thus, a continuous ET record was produced over the Northeast Asia domain for 2006 to 2008 by merging the MODIS ET and KLDAS ET records.

[31] The annual accumulated ET (hereafter, annual ET; mm yr^{-1}) showed a considerable spatial variation across the domain, with a mean and standard deviation of 362.0 mm yr^{-1} and 161.5 mm yr^{-1} for 2006 to 2008, and was generally higher at lower latitudes and elevations and in coastal and cropland regions (Figure 5). The annual ET for cropland dominated by irrigated paddy rice was generally high (445.7 ± 124.7 mm yr^{-1}) and represented the highest ET rates in southeastern China, an area where multiple cropping is widespread [*Xiao et al.*, 2005]. In contrast, grassland areas showed the lowest annual ET (193.6 ± 83.9 mm yr^{-1}) relative to the other land cover types (Table 5).

[32] Time series plots of the integrated MODIS-KLDAS ET and flux tower measurements at the GDK and HFK sites for 2006 are presented in Figure 6. The MODIS-KLDAS ET results generally track the seasonal course of measured ET at the two sites, including ET depressions during the summer monsoon period (Figure 6). The annual ET result was

Table 5. Mean and Standard Deviation of the Annual ET (mm yr^{-1}) for Individual Land Cover Types Within the Study Domain From 2006 to 2008

Land Cover	ET (mm yr^{-1})	SD	Maximum	Number of Pixels
ENF	377.2	129.8	889.7	81,078
EBF	745.1	122.8	1,022.43	20,838
DNF	318.5	56.4	614.0	21,091
DBF	466.2	59.4	895.6	180,095
MF	447.4	95.9	986.3	919,093
CSB	311.5	124.0	783.8	14,066
OSB	147.2	103.9	716.8	219,724
WSV	410.5	104.3	878.9	177,702
SV	326.0	100.4	857.6	54,882
GLD	193.6	83.9	822.2	1,188,444
PWD	423.6	126.7	1,069.4	5,918
CRP	445.7	124.7	938.8	1,556,908
CNV	497.2	107.9	861.1	39,037

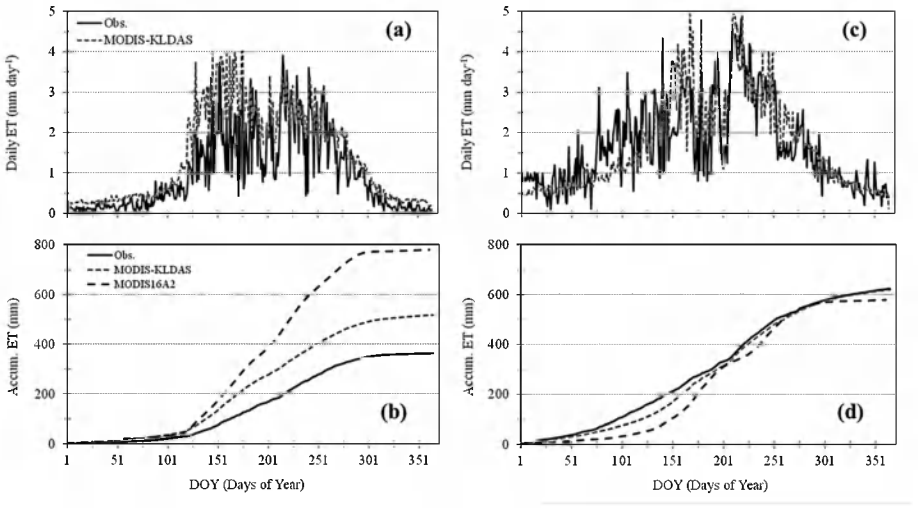

Figure 6. Time series and cumulative plots of the MODIS-KLDAS ET (dashed gray line), MODIS16A2 ET (dashed black line), and tower-measured ET (solid line) results at the (a and b) GDK and (c and d) HFK sites.

overestimated at the GDK site (Figures 6a and 6b). The MODIS-KLDAS ET results steeply increased earlier in spring (DOY 100–150) and showed higher values relative to the tower measurements. Although the overestimation pattern was sustained in early summer (DOY 180), MODIS-KLDAS ET paralleled the flux tower measurements after late summer (DOY 230). The annual ET for the GDK site was 517 mm and 367 mm for the model- and tower-based results, respectively, and MODIS-KLDAS ET at the GDK site showed a general overestimation of approximately 39.5% in 2006. For the HFK site, the MODIS-KLDAS result was underestimated when compared to the tower ET measurements until spring (DOY 150) and showed a similar range relative to the tower ET measurements after summer (Figure 6c). The resulting 2006 annual ET rates for the HFK site were 619 mm and 624 mm for the MODIS-KLDAS and tower results, respectively.

3.4. Comparison With the MODIS16 ET Product

[33] The MODIS-KLDAS ET results were compared to the MOD16A2 ET data to test model performance and compare relative spatial variability of the annual ET (mm yr^{-1}) results. Figure 7 shows the difference in annual ET between MOD16A2 and MODIS-KLDAS during the study period (2006–2008). In general, MODIS-KLDAS ET produced lower values than MOD16A2 ET, excluding cropland. In particular, the MOD16A2 ET values for the forest region, including the ENF, EDF, DNF, DBF, and MF biome types, were generally higher than our results. The MODIS-KLDAS annual ET values during the 3 years were relatively high for the cropland of southeastern and northeastern China and over western Korea. For both ET models, the lowest annual ET values in the study domain were found in the southern Mongolia and Inner Mongolia regions, which are dominated by grassland.

[34] The spatial variability of the difference in ET over complex terrain with relatively homogeneous land cover is shown in Figures 7a–7d. Figure 7a shows the ET difference over a cropland dominant area; the distribution of the ET difference was generally similar, though the MODIS-KLDAS ET results show strong variability in relation to topographic elevation. This pattern is also observed in other complex terrain areas within the domain (Figures 7b–7d). Furthermore, spatial variability of the difference in ET in relation to topographic aspect is also apparent. In the Changbai Mountains (Figure 7b), for example, the MODIS-KLDAS ET was higher than that of MOD16A2 ET for north and west facing slopes, whereas the MOD16A2 ET was higher for east facing slopes.

[35] The 8 day cumulative ET estimates from MODIS-KLDAS and MOD16A2 were compared with flux tower observations for 2006 at the GDK and HFK sites (see Figures 6b and 6d). Both models produced markedly overestimated results for the GDK site; ME (RMSE) for MODIS-KLDAS and MOD16A2 ET were +3.36 (4.68) mm 8 d^{-1} and +9.05 (13.41) mm 8 d^{-1}, and r^2 was 0.8876 and 0.9015, respectively. In contrast, a larger performance difference between the two models was noted for the HFK site. The MODIS-KLDAS ET results showed favorable agreement with the flux tower observations (ME = −0.09 mm 8 d^{-1}, RMSE = 3.46 mm 8 d^{-1}, $r^2 = 0.8386$), whereas the MOD16A2 ET showed generally lower correspondence (ME = −0.95 mm 8 d^{-1}, RMSE = 10.61 mm 8 d^{-1}, $r^2 = 0.3530$) at this site.

4. Discussion

[36] This study applied the methodology for ET estimation proposed by *Jang et al.* [2010] to monitor daily ET over Northeast Asia. We used a stand-alone MODIS ET algorithm [*Jang et al.*, 2010] under clear-sky and partially cloudy-sky conditions and applied the same algorithm using KLDAS meteorology and MODIS land products for cloudy conditions to facilitate continuous daily ET estimates. The stand-alone ET algorithm based on MODIS atmospheric and land products was used in this study and was evaluated using ground-based measurement data over Northeast Asia. In this study, the temporal resolution of the EVI data was improved from 16 days to 8 days by combining similar Terra and Aqua MODIS EVI products, which included the vegetation cover fraction in the calculation. In addition, the source of LAI

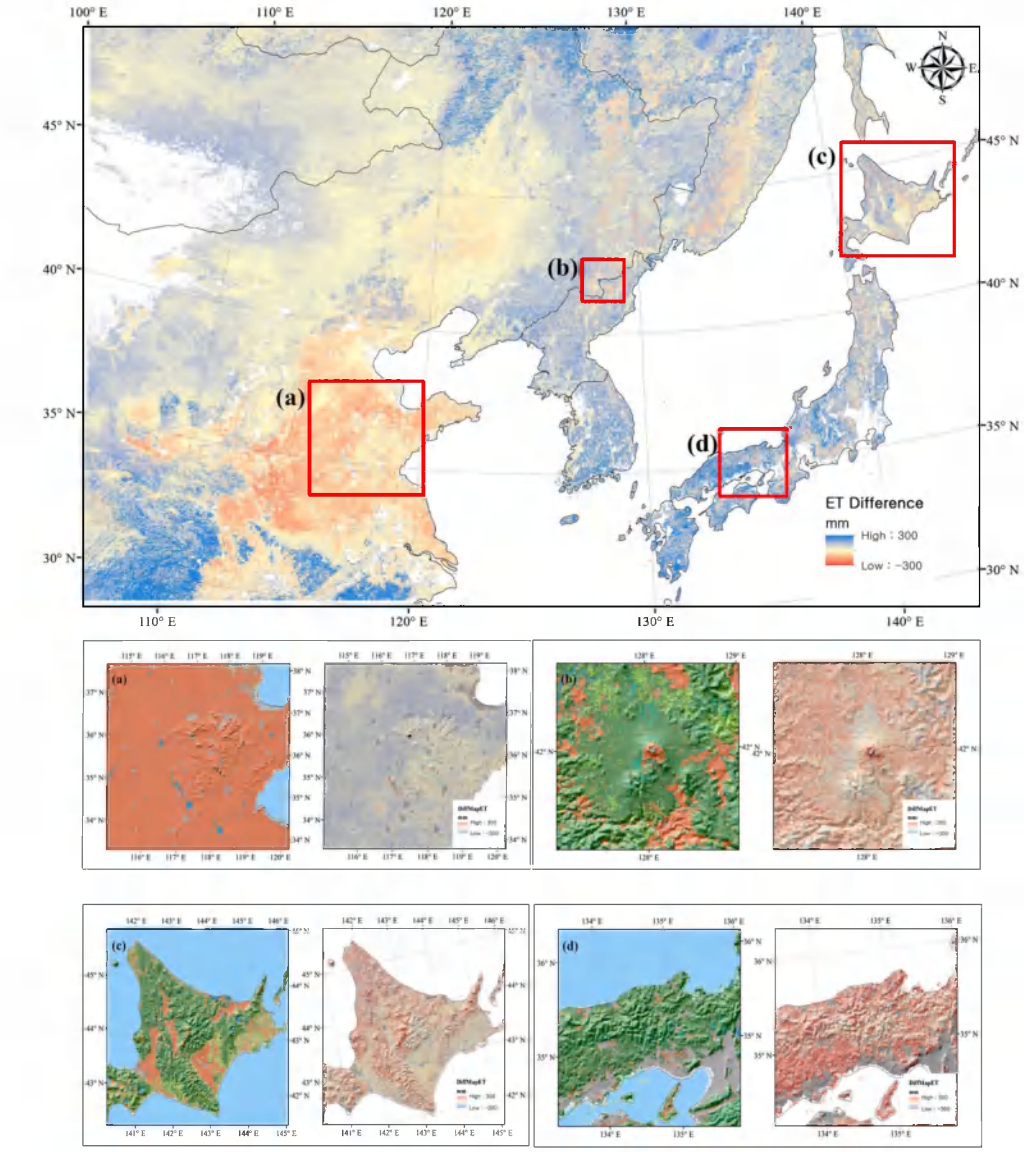

Figure 7. The map of annual ET differences between MOD16A2 and MODIS-KLDAS (MOD16A2 minus our results) from 2006 to 2008. The red boxes show the spatial variability of the differences in ET with regard to complex topography with relatively homogeneous land cover types in (a) the Shandong Peninsula, (b) the Changbai Mountains, (c) Hokkaido, and (d) the midwestern part of Japan (i.e., the Kansai region). Each box contains (left) the land cover map with (right) the digital elevation map and ET difference.

inputs from *Jang et al.* [2010] was changed by using the MYD15A2 product. The input meteorological variables derived from MODIS showed generally favorable agreement with the in situ measurements from flux tower sites within the study domain (Table 3). Despite the high accuracy of the MODIS input variables, the estimated ET showed considerable errors when compared to the tower observations at all sites (Figure 3 and Table 4). *Jang et al.* [2010] discussed the causes of such errors, including scale discrepancies between the relatively coarse 1 km spatial resolution of the MODIS grid cell compared to the local tower footprint and associated landscape heterogeneity, the coarse (8–16 day) temporal fidelity of the MODIS land products, and ET model parameter uncertainty, including canopy (or surface) and aerodynamic conductance terms.

[37] KLDAS ET was estimated using the KLDAS meteorology and MODIS land products. KLDAS DET showed a similar seasonal pattern to MODIS DET (not shown), because both ET models used similar methods except for surface meteorology inputs. The related errors of KLDAS DET at the GDK and HFK sites were slightly lower than the corresponding MODIS DET errors, which may attributed to differences in the number of available daily meteorological data used as ET model inputs. KLDAS meteorology was produced at hourly intervals and used to derive DET, while MODIS DET was generated from a single instantaneous ET (IET) retrieval over each pixel within the study domain. Thus, the diurnal ET variation may be better represented by the KLDAS DET, relative to MODIS DET estimated from the IET retrieval using a sinusoidal model.

[38] A model framework was developed and successfully tested for continuous spatiotemporal mapping of ET on a daily basis over the Northeast Asian region. The ET results for 3 years (2006–2008) were produced by integrating MODIS and KLDAS-driven ET calculations under clear-sky and cloudy-sky conditions. Overall, the ET results showed distinct spatial variations among the different regional biome types delineated by the MODIS (MOD12Q1) land cover classification. The integrated MODIS-KLDAS ET results showed relatively high values for forests, including evergreen broadleaf forest, deciduous broadleaf forest, mixed forest and croplands, and low values for grassland and open shrubland areas (Table 5). The ET results also showed large variability within the individual biome types that varied along latitudinal and elevation gradients. In particular, large ET gradients were evident for croplands from southeastern to northeastern China, in forests across the Korean Peninsula, and for coastal regions in Japan (Figure 5). The MODIS-KLDAS ET results were compared to tower measured ET at the GDK and HFK sites in South Korea and generally tracked the seasonal course of ET measurements at the two sites. The annual ET was overestimated by approximately 39.5% for the GDK (forest) site and underestimated by 0.8% for the HFK (cropland) site (Figures 6b and 6d). With regard to seasonal patterns, we observed considerable model-tower mismatches from the early spring to early summer seasons (Figures 6a and 6c), which may be due to uncertainty in springtime LAI and vegetation fractions.

[39] The MODIS-KLDAS ET results were compared against daily ET estimates from the MODIS MOD16A2 global product [*Mu et al.*, 2011], with the MODIS-KLDAS results showing higher ET levels in cropland regions, but lower ET levels in the other biome areas (Figure 7). Such discrepancies may be caused by considering the sheltering effect (f_s) on canopy conductance, using different maximum leaf conductance terms (C_L) for each biome type, and applying finer-scale regional meteorological data in the MODIS-KLDAS product. The shelter factor, f_s, which takes into account the shading effect caused by phenological changes [*Dingman*, 1994], was used in the calculation of the canopy conductance term, as suggested by *Jang et al.* [2010]; it plays an important role in reducing the canopy conductance at higher canopy densities (LAI$\geq$3). Consequently, the MODIS-KLDAS results showed lower ET levels than the MOD16A2 product, particularly for forested areas, and better agreement with tower ET measurements at a representative forest site (GDK). In addition, the effect of f_s for cropland ET is relatively lower than forest because of the generally smaller crop LAI levels. The utilization of different maximum leaf conductance (C_L) results explains the higher MODIS-KLDAS ET values found in crop regions compared to MOD16A2 ET. MOD16A2 ET uses the crop biome C_L of $0.0070\,\mathrm{m\,s^{-1}}$ [*Mu et al.*, 2011], whereas MODIS-KLDAS ET applies a value of $0.0110\,\mathrm{m\,s^{-1}}$ [*Federer et al.*, 1996; *Jang et al.*, 2010]. Another potential cause of the spatial discrepancy between MOD16A2 and MODIS-KLDAS ET is the use of different meteorological input variables. The MOD16A2 ET used GMAO ($1.00° \times 1.25°$) daily meteorological data as model inputs, whereas this study applied finer-scale (10 km resolution) KLDAS meteorological data and 5 km resolution MODIS data as primary model inputs. As *Kim et al.* [2012] noted, coarse GMAO meteorology is unable to capture finer-scale spatial variations in surface meteorology affected by complex topography and land cover conditions. Consequently, the MODIS-KLDAS results were able to capture spatial ET variability in relation to regional elevation gradients and topographic aspects within relatively homogeneous land cover areas (Figures 7a–7d).

[40] In this study, we demonstrated the integration of satellite (MODIS) remote sensing and mesoscale meteorological model (KLDAS) data for continuous regional monitoring of ET. Our integration method was successfully applied over the Northeast Asia region, an area where frequent and extensive cloud cover degrades satellite optical-infrared remote sensing capability, particularly during the summer monsoon period. We expect our integration method can be applied to any region with available regional meteorological data, though model accuracy will vary with regional differences in model input uncertainty and environmental conditions. Thus, model ET accuracy derived from meteorological inputs over regions with sparse observation network data could be lower than that in areas with better constrained meteorological forcing data. In addition, appropriate regional meteorological data may not exist for a specific research domain. For these reasons, there have been some efforts to estimate surface meteorology and ET based on stand-alone satellite remote sensing methods. Indeed, alternative methods have been developed for estimating the ET and radiation components solely from satellite remote sensing data [*Kim and Hogue*, 2008; *Wang and Liang*, 2009; *Wang and Pinker*, 2009; *Bisht and Bras*, 2010; *Vinukollu et al.*, 2011]. The development of new methods for estimating land surface radiant fluxes and ET from satellite data for all-sky conditions can provide an opportunity to overcome some of the limitations of the integration methods demonstrated in this study. This advance would enable truly independent satellite remote sensing-based ET retrievals without offline meteorological data for any region in the world.

[41] **Acknowledgments.** This research was supported by grants from the Sustainable Water Resources Research Center of the 21st Century Frontier Research Program (grant 1-8-3), Establishing an Assessment System for Crop Production and Agricultural Environment Using Remote Sensing from the Agenda Project of RDA, the A3 Foresight Program (CarboEastAsia) of KRF, TERRECO project of Ministry of Education, Science, and Technology (2011–0032202), Republic of Korea, and the NASA Terrestrial Hydrology program.

References

Alados, I., I. Foyo-Moreno, F. J. Olmo, and L. Alados-Arboledas (2003), Relationship between net radiation and solar radiation for semi-arid shrub-land, *Agric. For. Meteorol.*, *116*, 221–227.

Bastiaanssen, W. G. M., M. Menenti, R. A. Feddes, and A. A. M. Holtslag (1998), A remote sensing surface energy balance algorithm for land (SEBAL). 1. Formulation, *J. Hydrol.*, *212–213*, 198–212.

Bastiaanssen, W. G. M., E. J. M. Noordman, H. Pelgrum, G. Davids, B. P. Thoreson, and R. G. Allen (2005), SEBAL model with remotely sensed data to improve water-resources management under actual field conditions, *J. Irrig. Drain. E.-ASCE*, *131*, 85–93.

Bisht, G., and R. L. Bras (2010), Estimation of net radiation from the MODIS data under all sky conditions: Southern Great Plains case study, *Remote Sens. Environ.*, *114*, 1522–1534.

Bisht, G., V. Venturini, S. Islam, and L. Jiang (2005), Estimation of the net radiation using MODIS (Moderate Resolution Imaging Spectroradiometer) data for clear sky days, *Remote Sens. Environ.*, *97*, 52–67.

Boegh, E., H. Soegaard, J. H. Christensen, C. B. Hasager, N. O. Jensen, N. W. Nielsen, and M. S. Rasmussen (2004), Combining weather prediction and remote sensing data for the calculation of

evapotranspiration rates: Application to Denmark, *Int. J. Remote Sens.*, *25*(13), 2553–2574.

Chen, S., J. Chen, G. Lin, W. Zhang, H. Miao, L. Wei, J. Huang, and X. Han (2009), Energy balance and partition in Inner Mongolia steppe ecosystems with different land use types, *Agric. For. Meteorol.*, *149*(11), 1800–1809.

Cleugh, H. A., R. Leuning, Q. Mu, and S. W. Running (2007), Regional evaporation estimates from flux tower and MODIS satellite data, *Remote Sens. Environ.*, *106*, 285–304.

Crago, R., and W. Brutsaert (1996), Daytime evaporation and the self-preservation of the evaporative fraction and the Bowen ratio, *J Hydrol.*, *178*, 241–255.

De Goncalves, L. G., G. W. Shuttleworth, E. J. Burke, P. Houser, D. L. Toll, M. Rodell, and K. Arsenault (2006), Toward a South American Land Data Assimilation System: Aspects of land surface model spin-up using the Simplified Simple Biosphere, *J Geophys. Res.*, *111*, D17110, doi:10.1029/2005JD006297.

Dingman, S. L. (1994), *Physical Hydrology*, 2nd ed., pp. 272–324, Prentice Hall, New Jersey.

Dudhia, J., D. Gill, K. Manning, W. Wang, C. Bruyere, S. Kelly, and K. Lackey (2005), PSU/NCAR mesoscale modeling system tutorial class notes and user's guide: MM5 modeling system version3. Mesoscale and Microscale Meteorology Division, National Center for Atmospheric Research; Section 8–20.

Ek, M. B., K. E. Mitchell, Y. Lin, E. Rogers, P. Grunmann, V. Koren, G. Gayno, and D. Tarpley (2003), Implementation of Noah land surface model advances in the National Centers for Environmental Prediction operational mesoscale Eta model, *J. Geophys. Res.*, *108*(D22), 8851, doi:10.1029/2002JD003296.

Federer, C. A., C. Vorosmarty, and B. Fekete (1996), Intercomparison of methods for calculating potential evaporation in regional and global water balance models, *Water Resour. Res.*, *32*(7), 2315–2321.

Ferguson, C. R., J. Sheffield, E. F. Wood, and H. Gao (2010), Quantifying uncertainty in a remote sensing-based estimate of evapotranspiration over continental USA, *Int. J. Remote Sens.*, *31*(14), 3821–3865.

Glenn, E. P., A. R. Huete, P. L. Nagler, K. K. Hirschboeck, and P. Brown (2007), Integrating remote sensing and ground methods to estimate evapotranspiration, *Crit. Rev. Plant Sci.*, *26*, 139–168.

Hirata, R., et al. (2008), Spatial distribution of carbon balance in forest ecosystems across East Asia, *Agric. For. Meteorol.*, *148*(5), 761–775.

Jang, K., S. Kang, H. Kim, and H. Kwon (2009), Evaluation of shortwave irradiance and evapotranspiration derived from Moderate Resolution Imaging Spectroradiometer (MODIS), *Asia-Pac. J Atmos. Sci.*, *45*(2), 233–246.

Jang, K., S. Kang, J. Kim, C. B. Lee, T. Kim, J. Kim, R. Hirata, and N. Saigusa (2010), Mapping evapotranspiration using MODIS and MM5 four-dimensional data assimilation, *Remote Sens. Environ.*, *114*(3), 657–673.

Jeong, S., K. Jang, S. Kang, J. Kim, H. Kondo, M. Gamo, J. Asanuma, N. Saigusa, S. Wang, and S. Han (2009), Evaluation of MODIS-derived evapotranspiration at the flux tower sites in East Asia, *Korean J Agric. For. Meteorol.*, *11*(4), 174–184.

Jones, H. G. (1992), *Plants and Microclimate: A Quantitative Approach to Environmental Plant Physiology*, 2nd ed., Cambridge Univ. Press, Cambridge.

Kalma, J. D., T. R. McVicar, and M. F. McCabe (2008), Estimating land surface evapotranspiration: A review of methods using remotely sensed surface temperature data, *Surv. Geophys.*, *29*, 421–469.

Kaminsky, W. P., and R. Dubayah (1997), Estimation of surface net radiation in the boreal forest and northern prairie from shortwave flux measurements, *J. Geophys. Res.*, *102*(D24), 29,707–29,716.

Kang, S., S. W. Running, M. Zhao, J. S. Kimball, and J. Glassy (2005), Improving continuity of MODIS terrestrial photosynthesis products using an interpolation scheme for cloudy pixels, *Int. J. Remote Sens.*, *26*(8), 1659–1676.

Kim, J., and T. S. Hogue (2008), Evaluation of a MODIS-based potential evapotranspiration product at the point scale, *J. Hydrometeorol.*, *9*(3), 444–460.

Kim, J., et al. (2006), HydroKorea and CarboKorea: Cross-scale studies of ecohydrology and biogeochemistry in a heterogeneous and complex forest catchment of Korea, *Ecol. Res.*, *21*, 881–889.

Kim, H. W., K. Hwang, Q. Mu, S. O. Lee, and M. Choi (2012), Validation of MODIS 16 global terrestrial evapotranspiration products in various climates and land cover types in Asia, *KSCE J. Civ. Eng.*, *16*(2), 229–238.

Kwon, H. (2009), Estimation of net radiation in three different plant functional types in Korea, *Korean J. Agric. For. Meteorol.*, *11*(2), 79–85.

Lee, H. C., J. Hong, C.-H. Cho, B. C. Choi, S.-N. Oh, and J. Kim (2003), Surface exchange of energy and carbon dioxide between the atmosphere and a farmland in Haenam, Korea, *Korean J Agric. For. Meteorol.*, *5*, 61–69.

Li, S.-G., J. Asanuma, A. Kotani, W. Eugster, G. Davaa, D. Oyunbaatar, and M. Sugita (2005), Year-round measurements of net ecosystem CO2 flux over a montane larch forest in Mongolia, *J. Geophys. Res.*, *110*, D09303, doi:10.1029/2004JD005453.

Li, Z.-L., R. Tang, Z. Wan, Y. Bi, C. Zhou, B. Tang, G. Yan, and X. Zhang (2009), A review of current methodologies for regional evapotranspiration estimation from remotely sensed data, *Sensors*, *9*, 3,801–3,853.

Lim, Y.-J., K.-Y. Byun, T.-Y. Lee, and J. Kim (2010), Evaluation of evapotranspiration estimation using Korea land data assimilation system, *Korean J. Agric. For. Meteorol.*, *12*(4), 298–306.

Lu, X., and Q. Zuang (2010), Evaluating evapotranspiration and water-use efficiency of terrestrial ecosystems in the conterminous United States using MODIS and AmeriFlux data, *Remote Sens. Environ.*, *114*, 1924–1939.

Mitchell, K., et al. (2004), The multi-institution North American Land Data Assimilation System (NLDAS): Utilizing multiple GCIP products and partners in a continental distributed hydrological modeling system, *J. Geophys. Res.*, *109*, D07S90, doi:10.1029/2003JD003823.

Monteith, J. L. (1965), Evaporation and environment, *The State and Movement of Water in Living Organisms*, *Symp. Soc. Exp. Biol.*, vol. *19*, pp. 205–234, Cambridge Univ. Press, Cambridge, UK.

Monteith, J. L., and H. M. Unsworth (1990), *Principles of Environmental Physics*, 2nd ed., pp. , Edward Arnold, London, UK.

Mu, Q., F. A. Heinsch, M. Zhao, and S. W. Running (2007), Development of a global evapotranspiration algorithm based on MODIS and global meteorology data, *Remote Sens. Environ.*, *111*(4), 519–536.

Mu, Q., L. A. Jones, J. S. Kimball, K. C. McDonald, and S. W. Running (2009), Satellite assessment of land surface evapotranspiration for the pan-arctic domain, *Water Resour. Res.*, *45*, W09420, doi:10.1029/2008WR007189.

Mu, Q., M. Zhao, and S. W. Running (2011), Improvements to a MODIS global terrestrial evapotranspiration algorithm, *Remote Sens. Environ.*, *115*(8), 1781–1800.

Nishida, K., R. R. Nemani, S. W. Running, and J. M. Glassy (2003), An operational remote sensing algorithm of land surface evaporation, *J. Geophys. Res.*, *108*(D9), 4270, doi:10.1029/2002JD002062.

Oki, T., and S. Kanae (2006), Global hydrological cycles and world water resources, *Science*, *313*, 1068–1072.

Penman, H. L. (1948), Natural evaporation from open water, bare soil, and grass, *Proc. Roy. Soc. London, Series A*, *193*(1032), 120–145.

Renzullo, L. J., D. J. Barrett, A. S. Marks, M. J. Hill, J. P. Guerschman, Q. Mu, and S. W. Running (2008), Multi-sensor model-data fusion for estimation of hydrologic and energy flux parameters, *Remote Sens. Environ.*, *112*, 1306–1319.

Rodell, M., et al. (2004), The Global Land Data Assimilation System, *Bull. Am. Meteorol. Soc.*, *85*, 381–394.

Ryu, Y., S. Kang, S. Moon, and J. Kim (2008), Evaluation of Moderate Resolution Imaging Spectroradiometer (MODIS) derived land surface radiation balance over complex terrain and heterogeneous landscape for clear sky days, *Agric. For. Meteorol.*, *148*(10), 1538–1552.

Saigusa, N., et al. (2008), Temporal and spatial variations in the seasonal patterns of CO2 flux in boreal, temperate, and tropical forest in East Asia, *Agric. For. Meteorol.*, *148*(5), 700–713.

Saigusa, N., et al. (2010), Impact of meteorological anomalies in the 2003 summer on gross primary productivity in East Asia, *Biogeosciences*, *7*, 641–655.

Sheffield, J., C. R. Ferguson, T. J. Troy, E. F. Wood, and M. F. McCabe (2009), Closing the terrestrial water budget from satellite remote sensing, *Geophys. Res. Lett.*, *36*, L07403, doi:10.1029/2009GL037338.

Shuttleworth, W. J., R. J. Gurney, A. Y. Hsu, and J. P. Ormsby (1989), FIFE, the variation on energy partition at surface flux sites, paper presented at Proc. IAHS Third Int. Assembly, IAHS, Washington, D. C.

Su, Z. (2002), The surface energy balance system (SEBS) for estimation of turbulent heat fluxes, *Hydrol. Earth Syst. Sci.*, *6*(1), 85–99.

Sugita, M., and W. Brutsaert (1991), Daily evaporation over a region from lower boundary-layer profiles measured with radiosondes, *Water Resour. Res.*, *27*(5), 747–752.

Tang, Q., S. Peterson, R. H. Cuenca, Y. Hasimoto, and D. P. Lettenmaier (2009), Satellite-based near-real-time estimation of irrigated crop water consumption, *J. Geophys. Res.*, *114*, D05114, doi:10.1029/2008JD010854.

Trenberth, K. E., L. Smith, T. Qian, A. Dai, and J. Fasullo (2007), Estimation of the global water budget and its annual cycle using observational and model data, *J. Hydrometeorol*, *8*, 758–769.

Venturini, V., S. Islam, and L. Rodriguez (2008), Estimation of evaporative fraction and evapotranspiration from MODIS products using a complementary based model, *Remote Sens. Environ.*, *112*(1), 132–141.

Vinukollu, R. K., E. F. Wood, C. R. Ferguson, and J. B. Fisher (2011), Global estimates of evapotranspiration for climate studies using multi-sensor remote sensing data: Evaluation of three process-based approaches, *Remote Sens. Environ.*, *115*(3), 801–823.

Wang, J., and K. P. Georgakakos (2007), Estimation of potential evapotranspiration in the mountainous Panama Canal watershed, *Hydrol. Process.*, *21*, 1901–1917.

Wang, K., and S. Liang (2009), Global atmospheric downward longwave radiation over land surface under all-sky conditions from 1973 to 2008, *J. Geophys. Res.*, *114*, D19101, doi:10.1029/2009JD011800.

Wang, H., and R. T. Pinker (2009), Shortwave radiative fluxes from MODISL Model development and implementation, *J. Geophys. Res.*, *114*, D20201, doi:10.1029/2008JD10442.

Xiao, X., S. Boles, J. Liu, D. Zhuang, S. Frolking, C. Li, W. Salas, and B. Moore III (2005), Mapping paddy rice agriculture in southern China using multi-temporal MODIS images, *Remote Sens. Environ.*, *95*, 480–492.

Yang, F., M. A. White, A. R. Michaelis, K. Ichii, H. Hasimoto, P. Votava, A.-X. Zhu, and R. R. Nemani (2006), Prediction of continental-scale evapotranspiration by combining MODIS and AmeriFlux data through support vector machine, *IEEE Trans. Geosci. Remote Sens.*, *44*(11), 3452–3461.

Yu, G., X. Song, Q. Wang, Y. Liu, D. Guan, J. Yan, X. Sun, L. Zhang, and X. Wen (2007), Water-use efficiency of forest ecosystems in eastern China and its relations to climatic variables, *New Phytol.*, *177*, 927–937.

Yu, G.-R., et al. (2008), Environmental controls over carbon exchange of three forest ecosystems in eastern China, *Global Change Biol.*, *14*, 2555–2571.

Yuan, W., et al. (2010), Global estimates of evapotranspiration and gross primary production based on MODIS and global meteorology data, *Remote Sens. Environ.*, *114*(7), 1416–1431.

Zhang, K., J. S. Kimball, Q. Mu, L. A. Jones, S. J. Goetz, and S. W. Running (2009), Satellite based analysis of northern ET trends and associated changed in the regional water balance from 1983–2005, *J Hydrol.*, *379*, 92–110.

Zhao, M., and S. W. Running (2010), Drought-induced reduction in global terrestrial net primary production from 2000 through 2009, *Science*, *329*, 940–943.

Zhao, M., F. A. Heinsch, R. R. Nemani, and S. W. Running (2005), Improvements of the MODIS terrestrial gross and net primary production global data set, *Remote Sens. Environ.*, *95*, 164–176.

Zhongmin, H., et al. (2009), Partitioning of evapotranspiration and its controls in four grassland ecosystems: Application of a two-source model, *Agric. For. Meteorol.*, *149*, 1,410–1,420.